LBL-17391 c.2

Lawrence Berkeley Laboratory

UNIVERSITY OF CALIFORNIA

LAWRENCE
BERKELEY LABORATORY
MAR 12 1984
LIBRARY AND
DOCUMENTS SECTION

APPLIED SCIENCE DIVISION

To be presented at the XXth Symposium (International) on Combustion, Ann Arbor, MI, August 12-17, 1984

SOOT GENERATION WITHIN RADIATING DIFFUSION FLAMES

P.J. Pagni and C.I. Okoh

February 1984

TWO-WEEK LOAN COPY

This is a Library Circulating Copy which may be borrowed for two weeks. For a personal retention copy, call Tech. Info. Division, Ext. 6782.

APPLIED SCIENCE DIVISION

Prepared for the U.S. Department of Energy under Contract DE-AC03-76SF00098

LBL-17391 c.2

DISCLAIMER

This document was prepared as an account of work sponsored by the United States Government. While this document is believed to contain correct information, neither the United States Government nor any agency thereof, nor the Regents of the University of California, nor any of their employees, makes any warranty, express or implied, or assumes any legal responsibility for the accuracy, completeness, or usefulness of any information, apparatus, product, or process disclosed, or represents that its use would not infringe privately owned rights. Reference herein to any specific commercial product, process, or service by its trade name, trademark, manufacturer, or otherwise, does not necessarily constitute or imply its endorsement, recommendation, or favoring by the United States Government or any agency thereof, or the Regents of the University of California. The views and opinions of authors expressed herein do not necessarily state or reflect those of the United States Government or any agency thereof or the Regents of the University of California.

SOOT GENERATION WITHIN RADIATING DIFFUSION FLAMES

by

P.J. Pagni and C.I. Okoh

Mechanical Engineering Department

University of California

Berkeley, CA. 94720

and

Division of Applied Sciences

Lawrence Berkeley Laboratory

University of California

Berkerley, CA. 94720

Keywords

(4) Fires

(41) Soot Formation

(6) Heat Transfer and Radiation

Abstract

Soot volume fraction data on six fuels [C_7H_8, C_6H_{10}, C_8H_{18}, C_6H_{12}, C_7H_{16} and $(C_5H_8O_2)_n$] in free, radiating, boundary layer, diffusion flames are represented analytically. Approximate particle concentrations and size distributions, determined with previously reported optical techniques, are used. These sizes, $r \sim 30$ nm, indicate the particles are in the free molecular flow regime, $Kn \sim 10$, so that the thermal boundary layer thickness around the particle approaches zero and the particle temperature is locked to the local gas temperature. Based on this coupling and the experimental soot $f_v \sim 1$ ppm, the optically thin approximation is valid for incorporating soot radiation in the gas boundary layer equations. The pertinent fields, i.e. temperature, velocity and species, are reported. Thermophoretic forces are included in particle trajectory calculations. The local soot mass flow rates within the boundary layer are derived and net soot mass generation rates are obtained for these well characterized laminar flames. An Arrenhius expression appears to suffice to describe the temperature dependence of the soot growth rate over a 400°K temperature range, $1950 < T < 2350K$. Toluene has $E_a = 108$ kcal/mole while all the other fuels examined have $E_a = 86$ kcal/mole, very close to $H_3C - C_6H_5$ and C-C bond energies, respectively. Consistent with the goal of fire radiation prediction, calculated temperatures and velocities were used to obtain these empirical energies. Temperature and velocity measurements are in progress. Future work will include mixed flow boundary layer systems where control over the free stream oxygen mass fraction in a combustion tunnel configuration provides greater flame stability and a wider temperature range.

Introduction

The growth rate of full scale fires and hence their hazard is primarily controlled by the rate of heat transfer from the flames (1). This heat transfer is in turn dominated by flame radiation (2). It has been shown that CO_2 and H_2O emission is negligible compared with soot emission (3) which is characterized by f_v, the fraction of the flame volume occupied by solid carbon particles (4). While much progress has been made in developing procedures for calculating flame radiation (5,6), it is not possible to predict f_v in fires because the soot formation and destruction mechanisms have not been quantified (7). It is therefore necessary to measure *in situ* flame carbon particles. Probe sampling techniques significantly perturb the flames so that the sampled particles are not representative of the undisturbed flames unless carefully designed free molecular skimmers are used (8). Because of these difficulties, several optical techniques have evolved for *in situ* detection of carbon particles (9-16). While a concensus is yet to be obtained concerning optical properties (17-21), size distribution forms (22), particle shape (23), agglomeration rates (24) and even extinction or scattering coefficients (14,15,25), it is apparent that optical techniques have some advantages over intrusive sampling.

In the following sections: the optical technique used is briefly described along with the f_v data, the particle temperature is shown to be identical with the local gas temperature, the variable fields around the particles are given, particle trajectories are calculated including thermophoretic effects, the soot mass flow and net generation rates are obtained, and a simple Arrhenius expression is shown to describe $\dot{f}_v$ over much of the soot region near the flame sheet.

Soot, Temperature, Velocity and Species Fields

Figure 1 shows a free boundary layer flame with the main zones of interest indicated. The data shown in Fig. 2 were obtained from a previously described multi-wavelength extinction technique (14-16) which assumes a Gauss size distribution with $\sigma/r_m = 1/2$, giving the well behaved two parameter form,

$$N(r) = N_o(13.5\ r^3/r_{max}^4)\ \exp(-3r/r_{max}) \tag{1}$$

which has been shown to agree well with other assumptions (14,22). Integration gives

$$f_v = 18.62\ N_o\ r_{max}^3 \tag{2}$$

The authors claim no great advantage for this technique over several good alternate methods (9-13). It has been suggested (19,20) that the old optical properties of Dalzell and Sarofim (18) are low by approximately 30% due to void fractions in their compressed soot samples. The new refractive indices of Lee and Tien (17), which are higher by ~ 30%, were used here in the full Mie extinction theory. Attempts to approximate the extinction coefficient usually overestimate f_v (14,15). The criticism (21) that Lee and Tien's optical properties do not hold in the ultraviolet is correct (26). However, this is an optional consequence of intentionally eliminating π electrons in their dispersion theory to significantly reduce the number of parameters. Their accuracy at longer wavelengths (15,17,26) is excellent since their optical properties are based on transmission and emission measurements for large C/H ratio *in situ* diffusion flame soot in the visible and infrared.

The volume fraction profiles shown in Fig. 2 are a small portion of the available data (27,28). At each point, a size distribution in the form of Eq. (1) has been obtained from ~ 300 laser extinction measurements at > 3 visible wavelengths. The largest source of error is the slight unsteady fluctuation

Table I Empirical Fits to Soot Volume Fraction Data As Given by Equation (3)

Fuel	x(cm)	a_0	a_1	a_2	a_3	y_i(mm)	y_o(mm)
Toluene	2	- 1.51	1.95	1.23	-0.26	0.8	5.6
(C_7H_8)	4	-35.6	32.5	-7.35	0.51	2.0	5.6
Cyclohexene	2	- 3.90	3.09	-0.43	0.006	2.1	4.7
(C_6H_{10})	4	- 1.60	0.80	0.17	-0.037	2.6	6.4
	6	- 7.43	5.30	-0.90	0.044	2.4	7.6
	8	- 6.83	4.82	-0.75	0.031	2.3	7.6
	10	-10.5	7.60	-1.37	0.074	3.0	7.0
Iso-Octane	2	- 3.23	2.35	-0.45	0.024	2.5	5.9
(C_8H_{18})	4	- 4.64	2.87	-0.42	0.013	2.8	6.4
	6	- 6.08	4.05	-0.69	0.033	2.7	7.0
	8	- 4.69	3.75	-0.72	0.040	2.2	7.7
Cyclohexane	2	- 4.82	3.69	-0.82	0.056	2.7	4.7
(C_6H_{12})	4	- 2.40	-2.29	0.80	-0.084	2.5	5.3
	6	- 1.31	0.87	-0.07	-0.004	2.5	6.9
	8	- 2.79	1.64	-0.19	-0.002	2.9	6.9
	10	- 4.25	2.39	-0.32	0.010	3.7	7.3
n-Heptane	2	- 9.14	7.64	-2.05	0.180	2.9	4.5
(C_7H_{16})	4	- 5.31	3.48	-0.68	0.042	3.6	6.0
	6	- 6.86	4.15	-0.75	0.042	3.4	6.6
	8	- 4.05	2.31	-0.34	0.014	3.4	6.9
	10	- 3.07	1.75	-0.24	0.009	3.3	7.1
Polymethyl-	4	- 0.79	1.00	-0.21	-0.0008	1.2	3.5
methacrylate	6	- 0.39	0.63	-0.10	-0.0062	0.8	4.1
($C_5H_8O_2)_n$	8	- 0.08	0.52	-0.13	0.0058	0.5	4.9
	10	- 0.10	0.56	-0.16	0.0117	0.8	3.9

of these free flames which give error bars on f_v of the order of the scatter shown (± 15%). Data in mixed-flow obtained in a combustion tunnel are more stable and therefore more accurate, but the analytic problem of a radiating, combusting, mixed-flow boundary layer has not yet been solved. Since the net soot generation calculations require a knowledge of the velocity and temperature fields, this report is restricted to free flows. All of the free f_v data is summarized by the cubic fits in Table I which lists the coefficients and limits for the expression,

$$f_v = \sum_{j=0}^{3} a_j y^j \ , \quad y_i < y < y_o \tag{3}$$

The fits smooth the data for use in the generation calculations. They also provide convenient presentation of the detailed profiles at 2 cm downstream increments throughout the boundary layer for all six fuels. The fuels for which few increments are given were either too sooty or too unstable to monitor in more detail.

The size data give most probable radii, 20 nm < r_{max} < 40 nm. Throughout the soot region the gas mean free path, λ, varies from 400 nm to 600 nm, so that the Knudsen numbers, $\lambda/2r$, vary from 5 to 15, all >> 1 and well within the free molecular regime. This has the important consequence of locking soot particle temperatures to the local gas temperatures. In free molecular flow, gas molecules have direct access to the surface and a thermal boundary layer around the particle cannot exist. This produces a limiting case of infinite Biot number, i.e. $\delta_s \to 0$ and $h \sim k_g/\delta_s \to \infty$ so that $Bi = hr/k_s \to \infty$. In addition, the particles are so small that their thermal inertia → 0. Thus the particles are strongly coupled energetically to the gas and local thermal equilibrium, i.e. $T_s = T_g$ within << 1%, exists. Quantitative calculations (28) using free molecular transport expressions (29) indicate: $h \sim 0$

(10^5 W/m^2°K) with a characteristic thermal relaxation time on the order of nanoseconds, and show that reasonable surface reactions cannot provide sufficient energy to cause T_s to deviate more than 1°K from T_g. This is strictly a consequence of a large Knudsen number and would not hold for larger particles such as found in coal powder combustion (30).

The fact that the soot temperature is the gas temperature permits inclusion of soot radiation in the gas energy equation. The particle concentrations, N_o in Eq. (1), are 0 (10^9 cm^{-3}), giving f_v of 0 (1 ppm) which results (28) in absorption coefficients, κ, of 0 (1 m^{-1}). These small scale systems are therefore optically thin, $\kappa\delta < 0.1$ everywhere, and the radiation term in the energy equation is greatly simplified. The solution to the full set of boundary layer equations has been reported (28). Of interest here are the temperature, species and velocity fields in the soot region, as exemplified by Fig. 3 for n-heptane at x = 8 cm in air. To obtain these physical coordinate plots from the similarity variable solutions, it is necessary to evaluate a $\rho\mu$ product, which is assumed constant in the analysis, by comparison with flame shape photos and experimental fuel pyrolysis rates. Here $\rho\mu = 5$ g^2/sm^4 emerged as adequate for all fuels tested.

The species profiles in Fig. 3 indicate that products diffuse to the surface, where $Y_{fw} = 0.82$, $Y_{nw} = 0.13$ and $Y_{pw} = 0.05$ are typical while at the flame $Y_f = Y_o = 0$, $Y_p = 0.3$ and $Y_n = 0.7$. Soot exists throughout the range $0 < Y_f < 0.3$ and 1700°K $< T <$ 2300°K. The temperature gradient is slightly larger on the fuel side of the soot region. The x-velocity peaks near the maximum in the soot volume fraction, well inside the flame as expected for low mass consumption number fuels (31). The y-velocity begins positively due to surface pyrolysis, crosses zero at the converging streamline near the inner

edge of the soot layer, peaks negatively at the flame due to the low gas density there and remains negative for $y > y_{f\ell}$ as required in free flow for mass conservation within the boundary layer. The v extremum is more than an order of magnitude less than the u extremum. The fact that v is negative in the soot layer dictates that the soot observed near the flame must have been generated there. So while detailed formation mechanisms are still unclear, they must be strongly operative at low fuel mass fractions with high temperatures. Particle initiation, presumably by 3-5 ring PAHs (32), occurs close to the flame. Some oxidation, partly by OH (33), and soot growth, presumably by C_2H_2 (34,35), may occur throughout the soot region. All the f_v data were obtained in the pyrolysis region where fields similar to Fig. 3 exist. Burnout of the soot primarily occurs in the post-pyrolysis region well downstream of the flowfield depicted in Figs. 1-3.

Thermophoresis, Trajectories and Generation Rates

The presence of strong transverse temperature gradients in the boundary layer gives rise to thermophoretic forces. Nondimensionalizing the force balance on the particle shows that the characteristic momentum relaxation time is of $O(10^{-8})$ sec, thus the force balance is quasi-steady. Equating the thermophoretic force on a soot particle of radius r in a temperature gradient ∇T given by Eq. (15) of Talbot (36) with the viscous force from his Eq. (11b) gives the particle velocity relative to the gas,

$$v_s - v_g = \frac{-2\,\nu\, C_2\left(\frac{k_g}{k_s} + C_1\,Kn\right)[1 + Kn(A + Be^{-CKn})]\nabla T/T}{(1 + 3\,C_3\,Kn)(1 + 2\,\frac{k_g}{k_s} + 2\,C_1\,Kn)} \quad . \qquad (4)$$

The constants (36) are $C_1 = 1.09$, $C_2 = 1.17$, $C_3 = 0.57$, $A = 0.60$, $B = 0.21$, $C = 0.44$. Due to the large value of $Kn \sim 10$, the conductivity ratio has a

negligible effect on the velocity lag. The downstream temperature gradients are so small and u so large that $u_s = u_g$ to within 10^{-2}%. Conversely, the transverse temperature gradients are large and $v_s - v_g$ is O(-2 cm/sec) while - 10 cm/sec < v_g < 5 cm/sec with the thermophoretic effect clearly dominating near the converging streamline.

Figure 4 traces the streamwise evolution of the particle trajectories, including the effects of thermophoresis, for an n-heptane flame in air. The solid horizontal line is the flame sheet, and experimental soot profiles have been superposed on the soot region at five x stations. The effects of particle motion on soot concentrations are illustrated. New soot exists nearest the flame. The soot profile peak is formed partly by convection, while the oldest particles accumulate toward the fuel surface. These observations are confirmed by particle size and concentration data (14-16,27,28).

An integral formulation is useful to obtain the net local soot generation in these boundary layer flames. Such an approach may minimize the effect of the optical technique assumptions. Soot mass conservation can be written as

$$\int_{cv} \sum_i \dot{m}'''_{si} \, d\mathcal{V} = \frac{\partial}{\partial t} \int_{cv} \rho_s f_v \, d\mathcal{V} + \int_{cs} (\rho_s f_v) \underline{v} \cdot d\underline{A} \qquad (5)$$

where ρ_s is the soot density, here taken as 1.8 gm/cm^3 (37), and i indexes all generation and destruction processes. The system is steady, so the first term on the right goes to zero. Now adopt a two-dimensional control volume bounded by the pyrolysing fuel surface, by planes normal to that surface at x_0 and x_1, and by the flame sheet. There is no contribution to the control surface integral from the fuel or flame surfaces since $f_v = 0$ there, so that the net soot generation is the difference in the flux through the x_1 and x_0 planes, i.e.,

Table II Activation Energies, Temperature Limits and Net Soot Generation Rates

Fuel and E_a (kcal/mole)	x(cm)	y_{min}(mm)	T_i(°K)	T_{min}(°K)	T_o(°K)	Soot Mass Flow Rate (mg/s)	Net Soot Generation Rate Per Meter of Downstream Distance (g/s•m)
Toluene	2	3.8	1000	2000	2400	59.6	3.0
(C_7H_8)	4		1300		2300	83.9	1.2
E_a = 108							
Cyclohexene	2	3.6	1600	2000	2300	6.7	0.34
(C_6H_{10})	4	4.2	1650	2050	2400	17.8	0.55
E_a = 86	6	4.5	1450	2000	2400	30.0	0.61
	8		1400		2400	38.8	0.44
Iso-Octane	2	3.3	1700	1900	2350	2.9	0.15
(C_8H_{18})	4	3.8	1650	1900	2350	7.7	0.24
E_a = 86	6	4.5	1500	1950	2350	13.3	0.28
	8		1300		2350	21.0	0.38
Cyclohexane	2	3.5	1800	2000	2300	1.3	0.07
(C_6H_{12})	4	4.0	1600	2000	2300	5.0	0.19
E_a = 86	6	4.4	1650	2000	2400	10.0	0.25
	8	4.7	1550	2000	2400	13.3	0.15
	10		1750		2350	15.4	0.11
n-Heptane	2	3.5	1900	2000	2300	0.6	0.03
(C_7H_{16})	4	4.0	1950	2000	2400	2.2	0.11
E_a = 87	6	4.1	1800	1950	2400	4.6	0.12
	8	4.2	1750	1900	2400	7.5	0.15
	10		1650		2350	9.8	0.12
Polymethyl-	4	2.4	1500	1750	2100	1.7	0.09
methacrylate	6	2.5	1200	1750	2150	3.2	0.08
($C_5H_8O_2)_n$	8		1200		2150	5.1	0.09
E_a = 85							

$$\int_{x_0}^{x_1}\int_0^{y_{f\ell}} \sum_i \dot{m}_{si}''' \, dy \, dx = \int_0^{y_{f\ell}(x)} \rho_s f_v(x,y) \, u(x,y) \, dy \Big|_{x_0}^{x_1} \tag{6}$$

The size dependent thermophoretic force is eliminated by the dot product and only the x-velocity enters this equation.

Table II, column 7, gives the soot mass flow rate in the boundary layer from the integral on the right of Eq. (6) at each x, assuming uniform flow for one meter normal to the x-y plane. A zero soot mass flow rate is assumed at x = 0. The last column gives the right side of Eq. (6) divided by the increment, $(x_1 - x_0) = 2$ cm, in g/s•m. Also listed in columns 4 and 6 of Table II are the calculated temperatures at the y_i and y_o listed in Table I. The lower temperatures are in regions where soot has been convected; soot generation probably does not occur below 1500°K (38).

It is hoped that the net generation rates can be calculated from global models for the individual terms on the left of Eq. (6). With this in mind, a simple Arrenhius function is postulated

$$\dot{m}_s''' = \rho_s \dot{f}_v = \rho_s \, A \exp(-E_a/RT) \, Y_f^{\,b} \, f_v^{\,a} \tag{7}$$

A range of a and b were considered and a = 0, b = 1 emerged as providing the best fit. The change in f_v between the x stations along an average particle trajectory gives $\dot{f}_v$ as

$$u_m \frac{\Delta f}{\Delta s} = Y_{fm} A \exp\left(-E_a/RT_m\right) \tag{8}$$

where Δs is the distance along trajectories which lie near constant y lines so that only small variations are averaged in u_m, Y_{fm} and T_m. The good agreement between the data and the functional form of Eq. (7) is shown by the linearity and tightness of the data in Fig. 5 for iso-octane and n-heptane. The temperature range of this fit is given over each increment in columns 5

and 6, $T_{max} \approx T_o$, of Table II. The physical range over which the Arrhenius form applies is listed in columns 2 and 3 with $y_{max} \approx y_o \approx y_{f\ell}$. The activation energies obtained from least square analyses are given in column one of Table II. The activation energies collapse to two classes based on fuel structure. Cyclohexene, cyclohexane, iso-octane, n-heptane and polymethylmethacrylate all have $E_a \sim 86$ kcal/mole, while toluene with its methyl group has an $E_a \sim 108$ kcal/mole. These energies, although high (25), are suggestive of the carbon-carbon single bond energy, 84 kcal/mole and the methyl-phenyl bond energy, 100 kcal/mole. Further work is required for an elementary interpretation of these intriguing empirical results.

Nearer the fuel surface, in the region containing older particles, the data deviate from the Arrhenius form, i.e., $\dot{f}_v$ is substantially larger than the fit at lower temperatures, suggesting different mechanisms may be operative. Net generation rates predicted using these E_a agree well with the values obtained from the flux balances shown in column 8 of Table II.

Conclusion

In summary, soot volume fraction data on six fuels [C_7H_8, C_6H_{10}, C_8H_{18}, C_6H_{12}, C_7H_{16} and $(C_5H_8O_2)_n$] in free, radiating, boundary-layer diffusion flames have been fit with analytic expressions. In addition to volume fraction data, approximate particle concentrations and size distributions were determined with optical techniques previously reported. These sizes, $r \sim 30$ nm, indicate the particles are in the free molecular flow regime, $Kn \sim 10$, so that the thermal boundary layer thickness around the particle $\delta_s \to 0$ and the particle temperature is locked to the local gas temperature. Based on this coupling and the experimental soot $f_v \sim 1$ ppm, the optically thin approximation is valid for incorporating the local particle radiation in the governing

boundary layer equations for the gas. All pertinent fields, i.e. temperature, velocity and species, were calculated (28).

Recently developed expressions for thermophoretic forces were used to find the particle trajectories. The local soot mass flux within the boundary layer was derived and the net soot mass generation rates were obtained for these well characterized diffusion flames. A simple Arrenhius expression appears to suffice to describe the temperature dependence of this mass generation rate. The activation energies obtained are high: 86 kcal/mole, approximately equal to the C-C bond strength, for iso-octane, cyclohexane, n-heptane and polymethylmethacrylate, and 108 kcal/mole, approximately equal to the H_5C_6-CH_3 bond strength, for toluene. This may suggest that breaking these bonds is a rate limiting step in soot generation. Consistent with the goal of fire radiation prediction, calculated temperatures and velocities were used to obtain these empirical fits. Encouraged by the success of this simple approximation, experimental temperatures and velocities are now being obtained. On the analytic side, the radiation model is being improved for use in mixed flow boundary layers. Excellent work at many universities and laboratories is now directed at the problem of soot formation. Perhaps the next step is to apply independently developed optical and sampling techniques to the same flame and compare results. The well characterized boundary layer diffusion flames described here and elsewhere (16,25,39) and the even simpler pre-mixed flame systems on flat flame burners (35,40) are prime candidate systems for a program of critical evaluation of experimental techniques.

Nomenclature

f_v	particulate carbon volume/flame volume
h	heat transfer coefficient
k	thermal conductivity
$\dot{m}'''$	volumetric mass generation rate
N_o	particle concentration
r	particle radius
T	temperature
u	x-direction velocity
v	y-direction velocity
x	streamwise direction coordinate
y	transverse direction coordinate
Y	mass fraction

Greek

κ	absorption coefficient
λ	mean free path
μ	viscosity
ν	kinematic viscosity
ρ	density
σ	standard deviation

Subscripts

f	fuel
fl	flame
g	gas
i	inside

m	mean
max	most probable
n	neutral
o	oxygen or outside
p	product
s	soot
w	fuel surface

Acknowledgements

This work was supported by the Center for Fire Research in the U.S.D.O.C. National Bureau of Standards under Grant No. NB 80 NAGE6839-3 which was administered by the U.S. Department of Energy through the Applied Sciences Division of the Lawrence Berkeley Laboratory under Contract No. DE-AC03-76SF00098. Valuable discussions with J. de Ris of Factory Mutual Research Corporation and R. Santoro and H. Baum of the National Bureau of Standards are appreciated.

References

1. Emmons, H.W.: Seventeenth Symposium (International) on Combustion, pp. 1101-1111, The Combustion Institute, 1979.

2. de Ris, J.: Seventeenth Symposium (International) on Combustion, pp. 1003-1116, The Combustion Institute, 1979.

3. Bard, S., Clow, K.H. and Pagni, P.J.: Comb. Sci. and Tech., 19, 141-150, 1979.

4. Yuen, W.W. and Tien, C.L.: Sixteenth Symposium (International) on Combustion, pp. 1481-1487, The Combustion Institute, 1977.

5. Hubbard, G.L. and Tien, C.L.: ASME J. of Heat Transfer, 100, 235-239, 1978.

6. Tien, C.L. and Lee, S.C.: Progress Energy Combustion Science, 8, pp. 41-59, 1982.

7. Wagner, H. Gg: Seventeenth Symposium (International) on Combustion, pp. 3-19, The Combustion Institute, 1979.

8. Wersborg, B.L.: Howard, J.B. and Williams, G.C.: Fourteenth Symposium (International) on Combustion, pp. 929-940, The Combustion Institute, 1973.

9. Santoro, R.J., Semerjian, H.B. and Dobbins, R.A.: Combustion and Flame, 51, 203-218, 1983.

10. D'Alessio, A.: in Particulate Carbon Formation During Combustion (D.C. Siegla and G.W. Smith, Eds.), p. 207-259, Plenum Press, 1981.

11. Jagoda, I.J., Prado, G. and Lahaye, J.: Combust. Flame, 37, 261-274, 1980.

12. Kent, J.H. and Wagner, H.G.: Eighteenth Symposium (International) on Combustion, pp. 1117-1124, The Combustion Institute, 1981.

13. Bockhorn, H., et al.: Nineteenth Symposium (International) on Combustion, pp. 1413-1420, The Combustion Institute, 1983.

14. Pagni, P.J. and Bard, S: Seventeenth Symposium (International) on Combustion, pp. 1017-1028, The Combustion Institute, 1979.

15. Bard, S. and Pagni, P.J.: ASME J. of Heat Transfer, 103, 357-362, 1981.

16. Beier, R.A. and Pagni, P.J.: ASME J. of Heat Transfer, 105, 159-165, 1983.

17. Lee, S.C. and Tien, C.L.: Eighteenth Symposium (International) on Combustion, p. 1159-1166, The Combustion Institute, 1981.

18. Dalzell, W.H. and Sarofim, A.F.: ASME J. of Heat Transfer, 91, 100-104, 1969.

19. Graham, S.C.: Comb. Sci. and Tech., 9, 159-163, 1974.

20. Chippet, S. and Gray, W.A.: Combust. Flame, 31, 149-159, 1978.

21. Menna, P. and D'Alessio, A.: Nineteenth Symposium (International) on Combustion, pp. 1421-1428, The Combustion Institute, 1983.

22. Lee, S.C., Yu, Q.Z. and Tien, C.L.: J. Quant. Spectrosc. Radiat. Trans., 27, pp. 387-396, 1982.

23. Lee, S.C. and Tien, C.L.: J. Quant. Spectrosc. Radiat. Trans., 29, pp. 259-265, 1983.

24. Baum, H.R. and Mulholland, G.W.: J. of Colloid and Interface Sci., 72, 1-12, 1979.

25. Vandsburger, U., Kennedy, I. and Glassman, I.: Sooting Counterflow Diffusion Flames with Varying Oxygen Index in press in the Emmons Special Issue of Comb. Sci. and Tech.

26. Tien, C.L.: private communication.

27. Beier, R.A. and Pagni, P.J.: Soot Volume Fraction Profiles in a Free Combusting Boundary Layer, Twentieth National Heat Transfer Conference, ASME Paper No. 81-HT-1, 1981.

28. Beier, R.A., Pagni, P.J. and Okoh, C.I.: Soot and Radiation in Combusting Boundary Layers in press in the Emmons Special Issue of Comb. Sci. and Tech.

29. Sherman, F.S.: in Rarefied Gas Dynamics (J.A. Laurmann, Ed.) Vol. II, pp. 228-260, Academic Press, 1963.

30. Mitchell, R.E. and McClean, W.J.: Nineteenth Symposium (International) on Combustion, pp. 1113-1122, The Combustion Institute, 1983.

31. Pagni, P.J.: Fire Safety J., 3, 273-285, 1981.

32. Mallard, W.G. and Smyth, K.C.: private communication.

33. Neoh, K.G., Howard, J.B. and Sarofim, A.F.: in Particulate Carbon Formation During Combustion, (D.C. Siegla and G.W. Smith, Eds.), PP. 261-282, Plenum Press, 1981.

34. Harris, S.J. and Weiner, A.M.: Comb. Sci. and Tech., 31, 155-167, 1983.

35. Harris, S.J. and Weiner, A.M.: Comb. Sci. and Tech., 32, 267-275, 1983; in press 1984.

36. Talbot, L.: in Rarefied Gas Dynamics (S.S. Fisher, Ed.) Part I Vol. 74, Progress in Astronautics and Aeronautics, pp. 467-488, AIAA, 1981.

37. Park, C. and Appleton, J.P.: Combust. Flame, 20, 369-379, 1973.

38. Glassman, I. and Yaccarino, P.: Eighteenth Symposium (International) on Combustion, pp. 1175-1183, The Combustion Institute, 1981.

39. Tsuji, H. and Yamaoka, I.: Twelfth Symposium (International) on Combustion, pp. 977-1005, The Combustion Institute, 1969.

40. Flower, W.L.: Optical Measurements of Soot Formation in Premixed Flames, Western States Section, The Combustion Institute, Fall Meeting Paper No. 82-67, 1982.

Figure Captions

Fig. 1 Schematic diagram of a steady, two-dimensional, laminar, radiating combusting, boundary layer flame with soot on a vertical pyrolyzing fuel slab.

Fig. 2 Experimental soot volume fraction profiles and cubic curve fits for several fuels in air at a downstream location of x = 8 cm: PMMA (▽), n-heptane (■), iso-octane (○), cyclohexene (△).

Fig. 3 n-heptane/air free flow boundary layer profiles at x = 8 cm for T, temperature; u, x-velocity; v, y-velocity; f_v, soot volume fraction; Y_f, fuel mass fraction; Y_o, oxygen mass fraction; Y_p, product mass fraction and Y_n, inert mass fraction.

Fig. 4 Calculated trajectories of soot particles detected at x = 2 cm, 4 cm, 6 cm, and 8 cm downstream locations for n-heptane in air. Experimental f_v profiles are superposed with a 0-1 ppm scale at each location. Note the accumulation of older particles at the fuel side of the soot region, while the flame side is all fresh particles. This is consistent with measured sizes and concentrations.

Fig. 5 The Arrhenius correlation of soot generation for iso-octane with E_a = 86 kcal/mole and n-heptane with E_a = 87 kcal/mole.

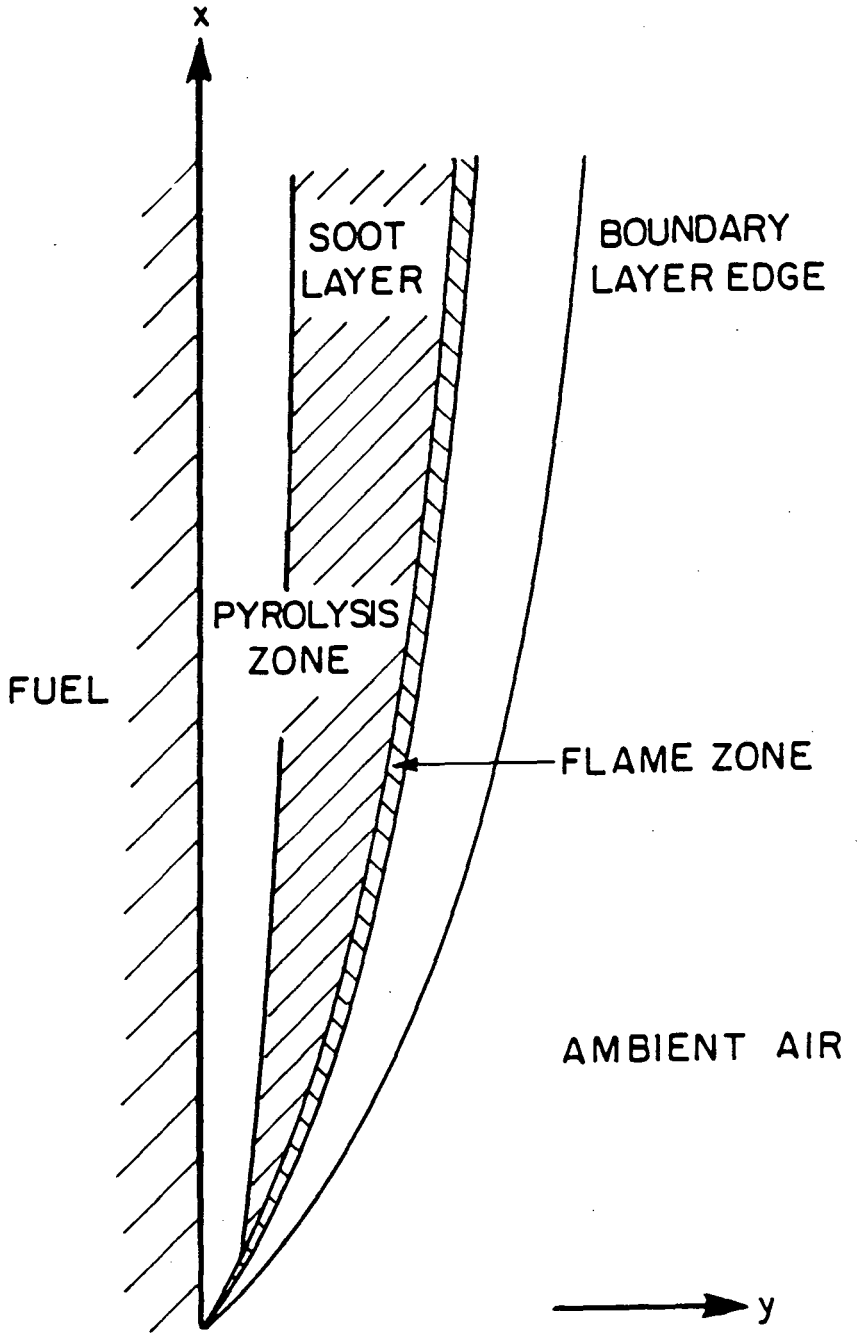

XBL 813-5397

Figure 1

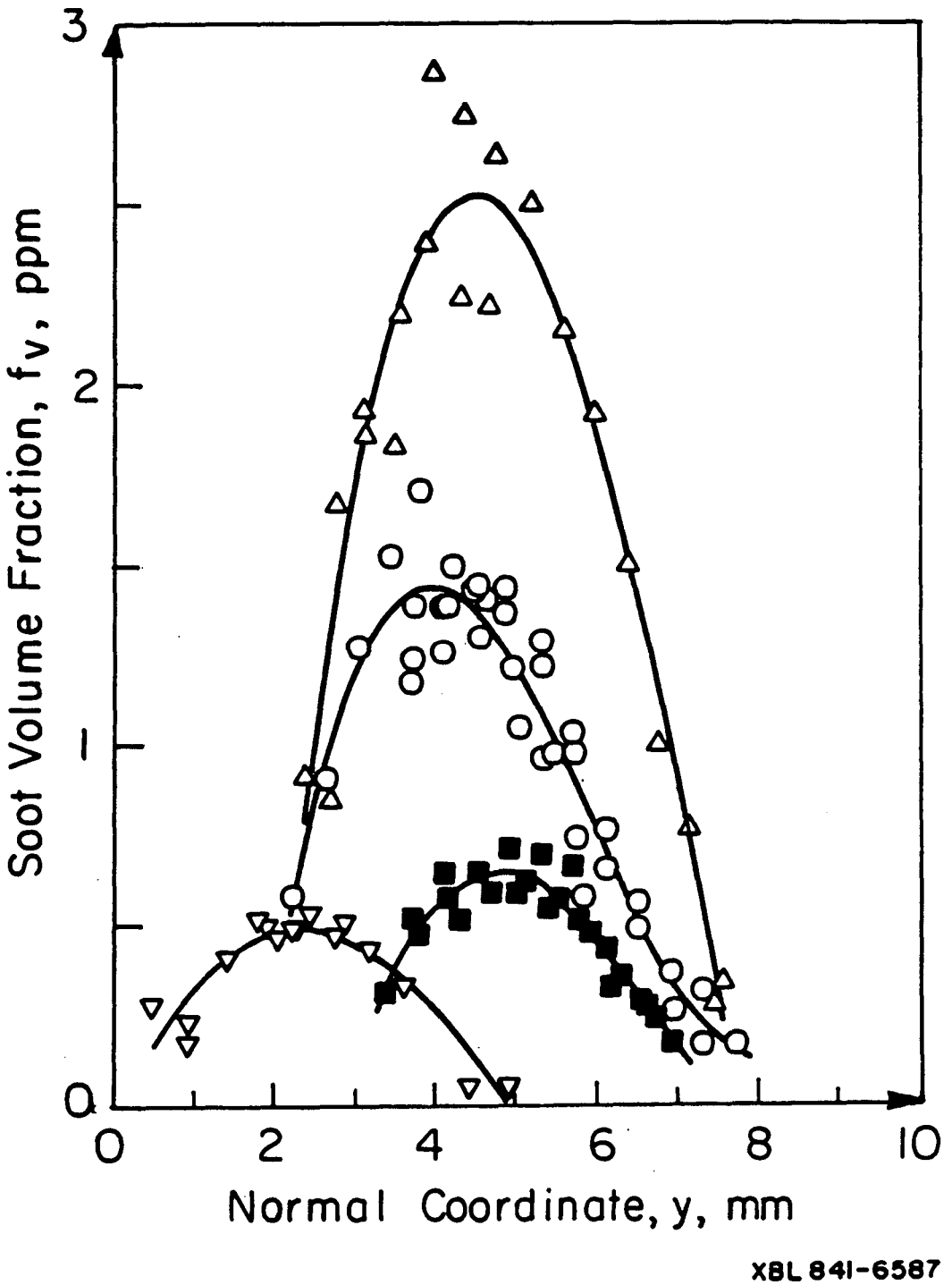
3
2
1
0
Soot Volume Fraction, f_v, ppm
0
2
4
6
8
10
Normal Coordinate, y, mm
XBL 841-6587

Figure 2

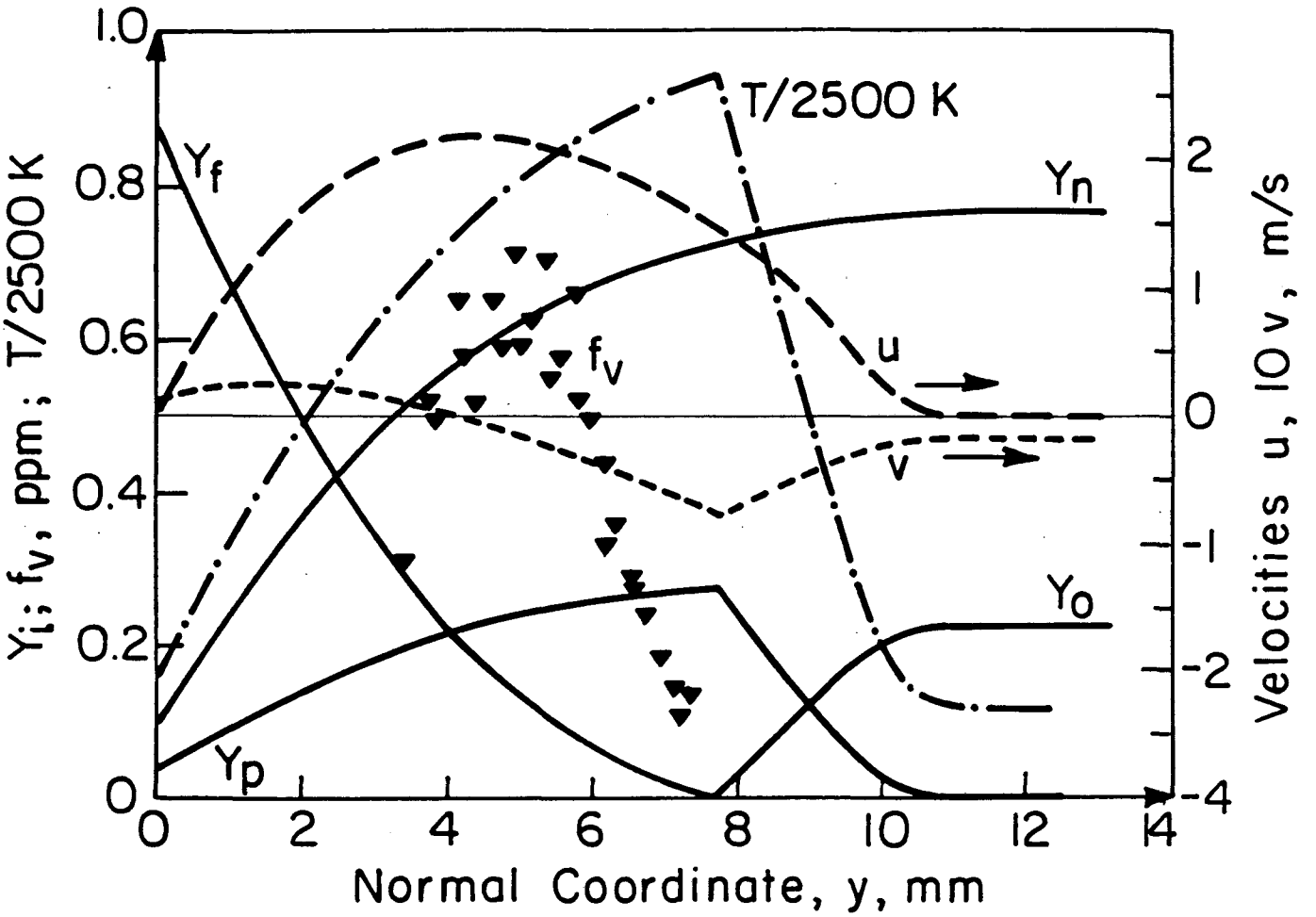

XBL 841-6589

Figure 3

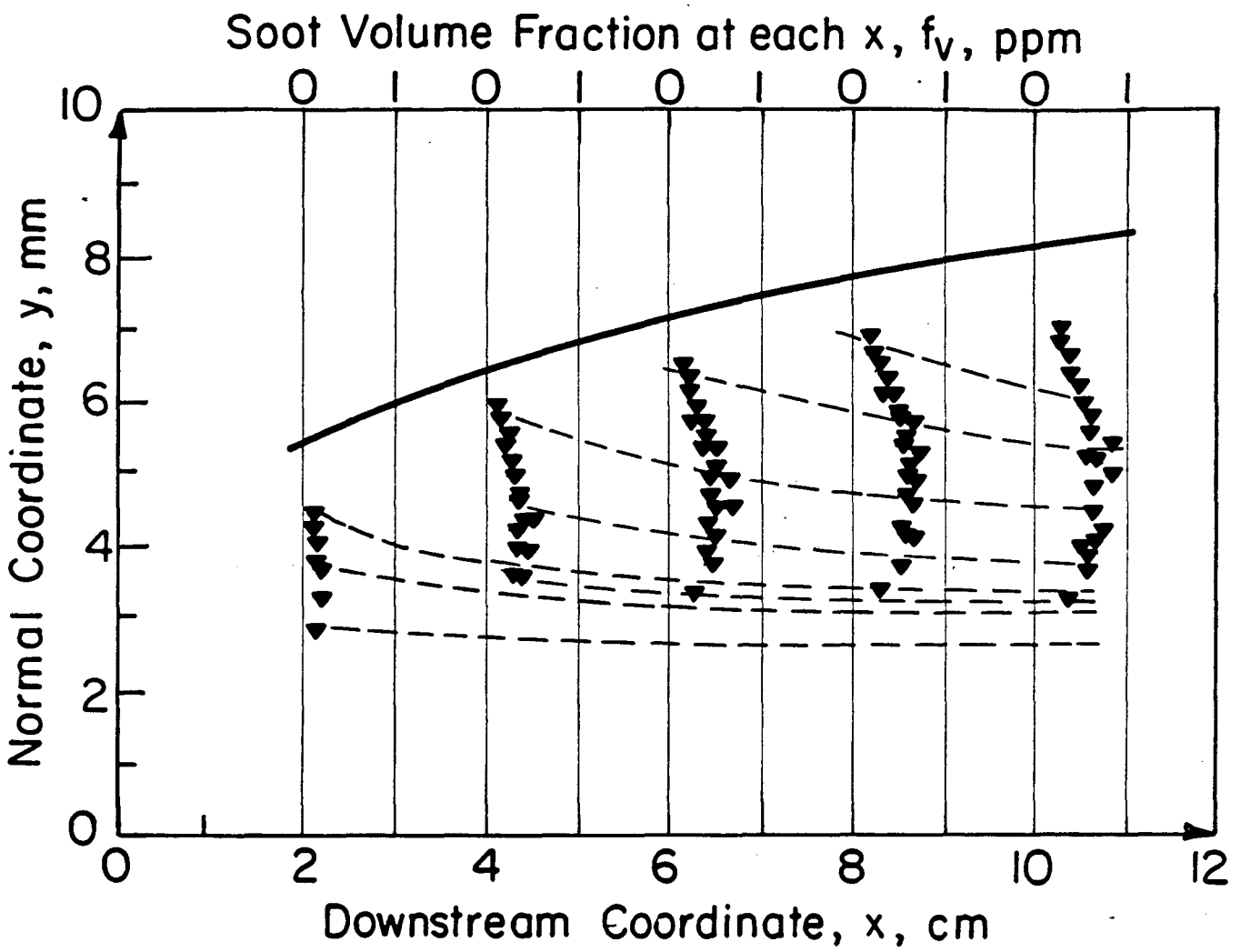

XBL 841-6588

Figure 4

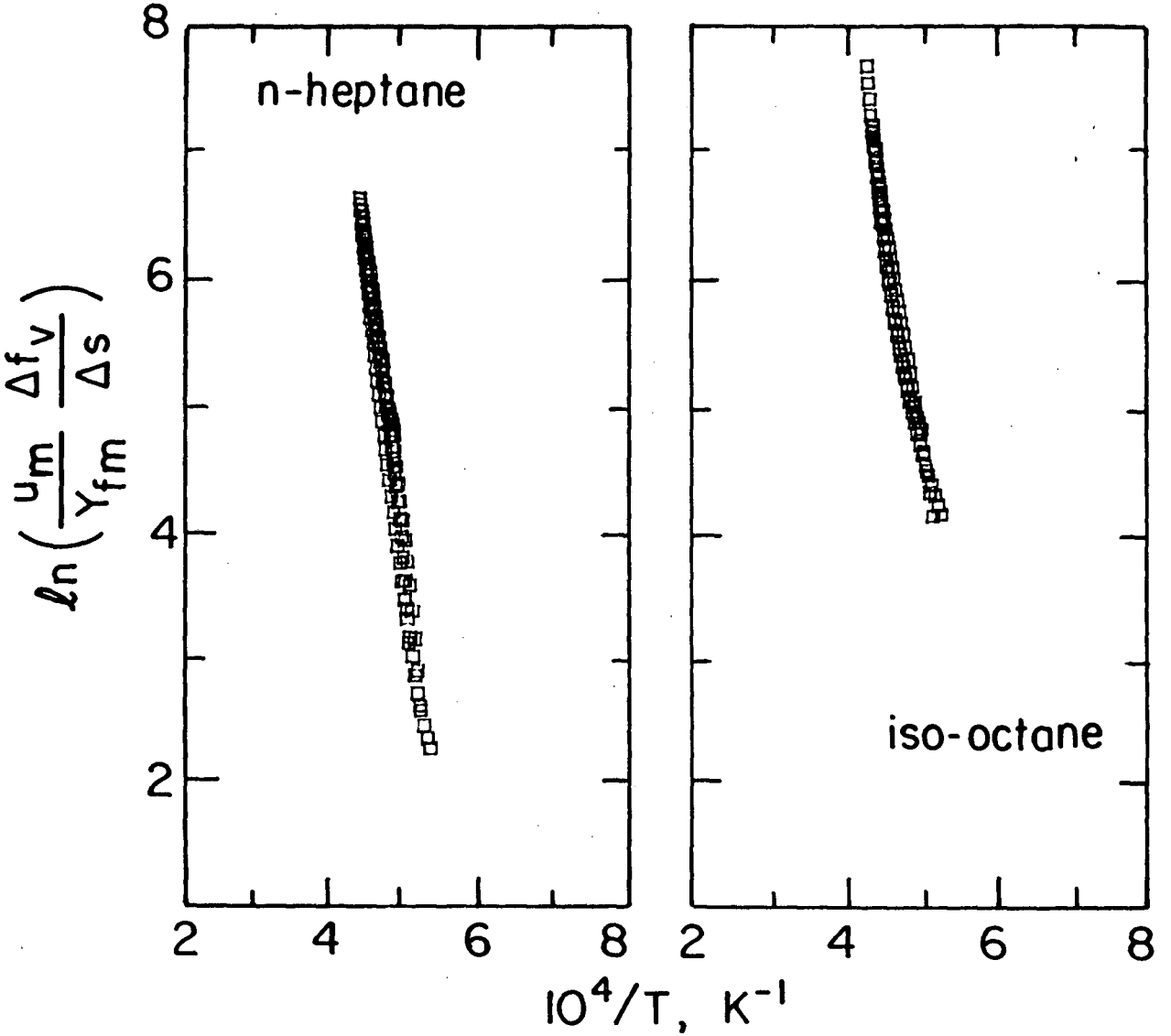

XBL 841-6590

Figure 5

5

This report was done with support from the Department of Energy. Any conclusions or opinions expressed in this report represent solely those of the author(s) and not necessarily those of The Regents of the University of California, the Lawrence Berkeley Laboratory or the Department of Energy.

Reference to a company or product name does not imply approval or recommendation of the product by the University of California or the U.S. Department of Energy to the exclusion of others that may be suitable.

TECHNICAL INFORMATION DEPARTMENT
LAWRENCE BERKELEY LABORATORY
UNIVERSITY OF CALIFORNIA
BERKELEY, CALIFORNIA 94720